Synthesis, Characterization, Catalytic Activity, and DFT Calculations of Zn(II) Hydrazone Complexes

Temiloluwa T. Adejumo [1], Nikolaos V. Tzouras [2], Leandros P. Zorba [2], Dušanka Radanović [3], Andrej Pevec [4], Sonja Grubišić [3], Dragana Mitić [5], Katarina K. Anđelković [1], Georgios C. Vougioukalakis [2,*], Božidar Čobeljić [1,*] and Iztok Turel [4,*]

[1] Faculty of Chemistry, University of Belgrade, Studentski trg 12–16, 11000 Belgrade, Serbia; adejumo.temiloluwa@gmail.com (T.T.A.); kka@chem.bg.ac.rs (K.K.A.)

[2] Laboratory of Organic Chemistry, Department of Chemistry, National and Kapodistrian University of Athens, Panepistimiopolis, 15771 Athens, Greece; nitzouras@gmail.com (N.V.T.); leozor888@gmail.com (L.P.Z.)

[3] Center for Chemistry, ICTM, University of Belgrade, Njegoševa 12, P.O. Box 815, 11001 Belgrade, Serbia; radanovic@chem.bg.ac.rs (D.R.); sonja.grubisic38@gmail.com (S.G.)

[4] Faculty of Chemistry and Chemical Technology, University of Ljubljana, Večna pot 113, 1000 Ljubljana, Slovenia; Andrej.Pevec@fkkt.uni-lj.si

[5] Innovation Centre of Faculty of Chemistry, University of Belgrade, Studentski trg 12–16, 11000 Belgrade, Serbia; dmitic@chem.bg.ac.rs

* Correspondence: vougiouk@chem.uoa.gr (G.C.V.); bozidar@chem.bg.ac.rs (B.Č.); Iztok.Turel@fkkt.uni-lj.si (I.T.); Tel.: +30-210-727-4230 (G.C.V.); +381-69-262-8978 (B.Č.); +386-1-479-8525 (I.T.)

Abstract: Two new Zn(II) complexes with tridentate hydrazone-based ligands (condensation products of 2-acetylthiazole) were synthesized and characterized by infrared (IR) and nuclear magnetic resonance (NMR) spectroscopy and single crystal X-ray diffraction methods. The complexes **1**, **2** and recently synthesized [Zn**L**^{3}(NCS)$_2$] (**L**^{3} = (*E*)-*N*,*N*,*N*-trimethyl-2-oxo-2-(2-(1-(pyridin-2-yl)ethylidene)hydrazinyl)ethan-1-aminium) complex **3** were tested as potential catalysts for the ketone-amine-alkyne (KA^2) coupling reaction. The gas-phase geometry optimization of newly synthesized and characterized Zn(II) complexes has been computed at the density functional theory (DFT)/B3LYP/6–31G level of theory, while the highest occupied molecular orbital and lowest unoccupied molecular orbital (HOMO and LUMO) energies were calculated within the time-dependent density functional theory (TD-DFT) at B3LYP/6-31G and B3LYP/6-311G(d,p) levels of theory. From the energies of frontier molecular orbitals (HOMO–LUMO), the reactivity descriptors, such as chemical potential (μ), hardness (η), softness (S), electronegativity (χ) and electrophilicity index (ω) have been calculated. The energetic behavior of the investigated compounds (**1** and **2**) has been examined in gas phase and solvent media using the polarizable continuum model. For comparison reasons, the same calculations have been performed for recently synthesized [Zn**L**^{3}(NCS)$_2$] complex **3**. DFT results show that compound **1** has the smaller frontier orbital gap so, it is more polarizable and is associated with a higher chemical reactivity, low kinetic stability and is termed as soft molecule.

Keywords: Girard's T reagent; hydrazone ligand; Zn(II) complexes; XRD; ketone-amine-alkyne coupling reaction; catalysis; DFT calculation

1. Introduction

Hydrazone ligands are one of the most important classes of flexible and versatile polydentate ligands which show very high efficiency in chelating various metal ions [1–13]. The coordination behavior of hydrazones is known to depend on the pH of the medium, the nature of the

substituents and on the position of the hydrazone group relative to other moieties [2–4]. Moreover, deprotonation of the –NH group, which is readily achieved in the complexed ligand in particular, results in the formation of tautomeric anionic species (=N–N$^-$–C=O or =N–N=C–O$^-$), having different coordination properties. Our interest in metal complexes with hydrazone-based ligands is partly due to their potential applications as catalysts [5,6] and molecular magnets [7]. Hydrazone ligands, obtained from Girard's T reagent (trimethylammoniumacetohydrazide chloride) and 2-acetylpyridine or 2-quinolinecarboxaldehyde (**HL^3**Cl = (*E*)-*N*,*N*,*N*-trimethyl-2-oxo-2-(2-(1-(pyridin-2-yl)ethylidene)hydrazinyl)ethan-1-aminium chloride and **HL^4**Cl = (*E*)-*N*,*N*,*N*-trimethyl-2-oxo-2-(2-(quinolin-2-ylmethylene)hydrazinyl)ethan-1-aminium chloride) are tridentate ligands which show the potential to form mononuclear and binuclear structures with metal ions [3,4,6,8–10]. In the mononuclear complexes (e.g., [Zn**L^3**(NCS)$_2$] (**3**) [8], [Cd**HL^3**(NCS)$_2$(SCN)] [8], [Zn**L^4**(N$_3$)$_2$] [9], [Zn**L^4**(NCO)$_2$] [9], [Zn**L^4**(N$_3$)$_{1.65}$Cl$_{0.35}$] [10], [Cd**L^4**(NCO)$_{1.64}$Cl$_{0.36}$] [10] and [Co**HL^4**(N$_3$)$_3$] [4]) with one hydrazone ligand being coordinated in a tridentate fashion to the central metal ion, the vacant coordination sites are filled by monodentate ligands (pseudohalides/halides) and in some cases by counter anions of starting metal salts [11]. In the other type of mononuclear structures two hydrazone ligand molecules occupy the coordination sphere of the central metal ion forming an octahedral coordination geometry (e.g., [Co**L^3**$_2$][Co(NCS)$_4$]BF$_4$ [12] and Zn(II) complex with the 2-acetylthiazole (N4)-phenylthiosemicarbazone ligand (CCDC 1059843) [13]). In the binuclear [M$_2$(**L^4**)$_2$($\mu_{1,1}$-N$_3$)$_2$(N$_3$)$_2$]·H$_2$O·CH$_3$OH (M = Ni(II) and Co(II)) [3,4] and [Cu$_2$(**L^3**)$_2$($\mu_{1,1}$-N$_3$)$_2$](ClO$_4$)$_2$ [6] complexes, the hydrazone-based ligands show the same tridentate *N*,*N*,*O*-coordination mode forming the octahedral structure in the former two complexes cooperatively with two bridging and one terminal azide anion per metallic center and the square pyramidal in the latter with two bridging azides.

On the other hand, the propargylamines are a unique family of organic compounds, which has received ample attention by the wider scientific community [14,15]. The profound interest surrounding these compounds is partly due to the bioactive nature of certain members of their family [14–17]. Furthermore, propargylic amines are frequently encountered as intermediates in organic synthesis, providing facile access to a variety of structurally complex organic compounds [14,15]. Among these compounds, the subgroup of tetrasubstitutedpropargylamines is particularly interesting, as it comprises the least studied family of propargylamines. The most straightforward approach towards such molecules is the ketone-amine-alkyne (KA^2) multicomponent coupling reaction, for which a significant number of catalytic systems has been reported during the past decade [18–28]. As part of the work of some authors focusing on sustainable organic transformations, multicomponent reactions and sustainable metal catalysis [19–33], the first zinc-based homogeneous catalytic system for the KA^2 coupling was disclosed very recently [34]. Since the use of ligands in these catalytic systems is rare, we were interested in testing well-defined zinc complexes as potential catalysts for the reaction operating under air.

Herein, we report the synthesis and characterization of two new Zn(II) complexes [Zn**L^1**(NCS)$_2$]·2H$_2$O (**1**) and [Zn(**L^2**)$_2$] (**2**)with the condensation products of 2-acetylthiazole and trimethylammoniumacetohydrazide chloride (Girard's T reagent) and thiosemicarbazide, respectively. The structures of **1** and **2** were characterized by infrared (IR) and nuclear magnetic resonance (NMR) spectroscopy and single crystal X-ray diffraction methods. The catalytic activity of **1** and **2** and the previously characterized [Zn**L^3**(NCS)$_2$]·0.5MeOH [8] complex **3** has been evaluated in the ketone-amine-alkyne (KA^2) coupling reaction. The experimental studies on the catalytic activities of **1**, **2** and recently synthesized [Zn**L^3**(NCS)$_2$]·0.5MeOH [8] (**3**) complex have been accompanied by density functional theory (DFT) calculations. We used B3LYP, a density functional theory-based approach, to describe the structures and molecular properties of the compounds of interest. The global reactivity descriptors, namely, chemical potential (μ), hardness (η), softness (S), electronegativity (χ), and electrophilicity index (ω) have been evaluated from highest occupied molecular orbital (HOMO) and lowest unoccupied molecular orbital (LUMO) energy values.

2. Results and Discussion

2.1. Synthesis

The ligand (**HL^1**Cl), (*E*)-*N,N,N*-trimethyl-2-oxo-2-(2-(1-(thiazol-2-yl)ethylidene)hydrazinyl) ethan-1-aminium chloride, was obtained from the condensation reaction of 2-acetylthiazole and Girard's T reagent. By the reaction of ligand **HL^1**Cl with Zn(OAc)$_2$·4H$_2$O and NH$_4$SCN in excess in solvent mixture of water/methanol, mononuclear Zn(II) complex **1**, with the composition [ZnL^1(NCS)$_2$]·2H$_2$O, was obtained (Scheme 1a). In complex **1**, Zn(II) is pentacoordinated with the thiazole nitrogen, the azomethine nitrogen, and the carbonyl oxygen atoms from the deprotonated hydrazone ligand and two thiocyanate ligands coordinated through the nitrogen atoms. Reaction of ligand **HL^2** ((*E*)-2-(1-(thiazol-2-yl)ethylidene)hydrazine-1-carbothioamide) with Zn(BF$_4$)$_2$·6H$_2$O and NaN$_3$ in a 1:1:2.3 molar ratios, in a mixture of acetonitrile/water, gives mononuclear Zn(II) complex **2**, with composition [Zn(**L^2**)$_2$] (Scheme 1b). Two deprotonated ligands **L^2** are coordinated to Zn(II) ion through the thiazole nitrogen, the imine nitrogen, and the thiolate sulfur atoms, forming a distorted octahedral complex. Complex **3**, with composition [ZnL^3(NCS)$_2$]·0.5MeOH was previously reported [8] and has a similar structure to complex **1** (Scheme 1c).
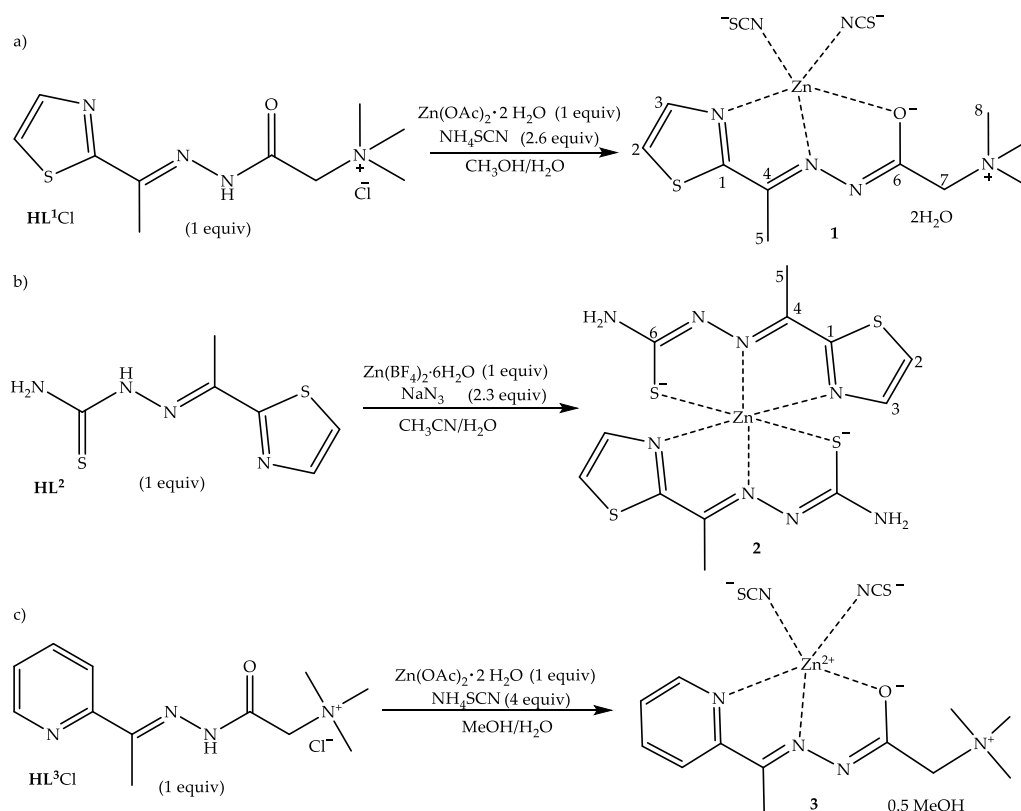
Scheme 1. Synthesis of: (**a**) [ZnL^1(NCS)$_2$]·2H$_2$O (**1**) complex; (**b**) [Zn(**L^2**)$_2$] (**2**) complex; (**c**) [ZnL^3(NCS)$_2$]·0.5MeOH (**3**) complex.

2.2. Crystal Structures of [ZnL^1(NCS)$_2$]·2H$_2$O (1) and [Zn(L^2)$_2$] (2) Complexes

The molecular structure of **1** is shown in Figure 1. Selected bond distances and angles are given in Table 1. The neutral complex [ZnL^1(NCS)$_2$] crystallizes as dihydrate in the triclinic crystal system with space group *P*−1. In **1**, Zn1 has fivefold coordination with tridentate ligand **L^1** and two nitrogen atoms (N5, N6) from thiocyanate ligands. **L^1** is coordinated to Zn1 in the zwitterionic form through NNO-set of donor atoms forming two fused five-membered chelate rings (Zn–N–C–C–N and Zn–N–N–C–O). The dihedral angle of nearly 4.0° between two five-membered chelate rings shows the non-coplanar

nature of metal-ligand system. Generally, the distortion in the five coordinated systems is described by an index of trigonality $\tau = (\beta - \alpha)/60$, where β is the greatest basal angle and α is the second greatest angle [35]. The parameter τ is 0 for regular square based pyramidal forms and 1 for trigonal bipyramidal forms. The τ value of 0.36 calculated for **1**, indicates that the irregular coordination geometry about Zn1 is 36% trigonally distorted square-based pyramidal. The greatest basal angles O1−Zn1−N1 and N2−Zn1−N5 are 149.20(7)° and 127.42(10)°, respectively. The Zn1 is lifted out of the plane of the four in-plane ligand atoms (O1, N1, N2 and N5) by a distance ρ of 0.6091(3) Å. The complex **1** shows slightly greater degree of trigonal distortion from ideal square-based pyramidal configuration, in comparison with the other five-coordinate Zn(II) complexes with *N*-heteroaromaticmonohydrazones of Girard's T reagent and pseudohalide or halide ligand (N_3^-, NCO^-, NCS^- or Cl^-) as monodentate for which the calculated τ values are in the range 0.31–0.34 (complexes **3–6**, Table S1 in the Supplementary Materials) [8–10]. The τ values for complexes **1**, **3–6** fit into the range of values obtained for related Zn(II)complexes [36–40] (complexes **7–15**, Table S1 in the Supplementary Materials). The Zn(II) ion in **1** is more strongly bound to the imine nitrogen atom of the ligand L^1 than to the 1,3-thiazole nitrogen, as indicated by the Zn1–N2, 2.058(2) Å and Zn1–N1, 2.212(2) Å bond lengths (Table 2). Similar to this, in analogous Zn(II) complexes with Girard's T hydrazone-based ligands and N_3^-, NCO^-, NCS^- or Cl^- as monodentate ligands [8–10] the Zn−N(imine), 2.049(3)–2.088(6) Å bond lengths are shorter than Zn–N(pyridine/quinoline), 2.206(6)/2.240(2)–2.344(2) Å bond lengths, indicating that Zn(II) ion is more tied to the imine nitrogen atom than to the pyridine or quinoline nitrogen atoms. In complexes **1**, **3–6**, the Zn−O(enolic) bond distances are in the range from 2.146(5) to 2.222(2) Å. The shortest Zn−O(enolic) bond length is found in the $[ZnL^3(NCS)_2]\cdot0.5MeOH$ [8] complex and the longest in $[ZnL^4(N_3)_{1.65}Cl_{0.35}]$ [10] (L^3 = condensation product of 2-acetylpyridine and trimethylammoniumacetohydrazide chloride and L^4 = condensation product of. 2-quinolinecarboxaldehyde and trimethylammoniumacetohydrazide chloride). The thiocyanate ligands in **1** are coordinated to Zn(II) ion in bent mode, with Zn−N−C angles of 168.5(3) and 171.7(2)°. In the crystals of **1** the complex molecules $[ZnL^1(NCS)_2]$ are assembled into supramolecular layers parallel with the (0 0 1) lattice plane by means of moderate O1W–H1W⋯O1 and weak C8–H8A⋯S2 and C10–H10B⋯O1W intermolecular hydrogen bonds [41] (Table S2, Figure S1a in the Supplementary Materials). In addition, the solvent water molecules O1W and O2W assists in joining the neighboring layers related by the center of symmetry by means of weak intermolecular hydrogen bonds C–H⋯OW (Table S2, Figure S2b in the Supplementary Materials). The shortest separations of 4.467(2) and 4.666(2) Å between the centers of gravity of the 1,3-thiazole rings are observed along the [−1 1 0] direction.
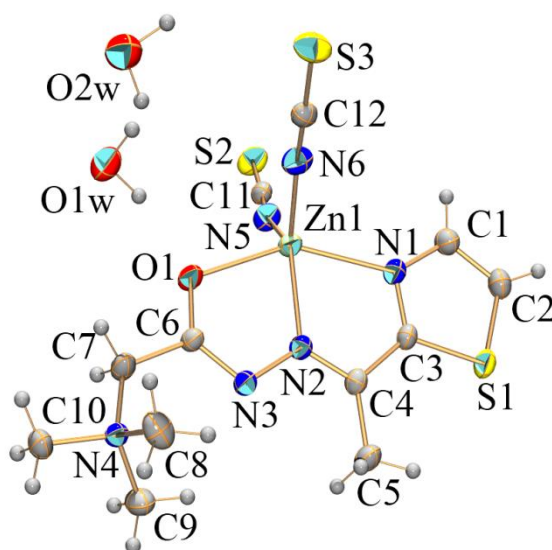

Figure 1. ORTEP presentation of the molecular structure of $[ZnL^1(NCS)_2]\cdot2H_2O$ (**1**). Thermal ellipsoids are drawn at the 30% probability level.

Table 1. Selected bond lengths (Å) and angles (°) for **1** and **2**.

1		**2**	
Zn1–N6	1.955(3)	Zn1–N6	2.149(2)
Zn1–N5	1.959(2)	Zn1–N5	2.1869(19)
Zn1–N2	2.058(2)	Zn1–N2	2.147(2)
Zn1–O1	2.1778(19)	Zn1–N1	2.318(2)
Zn1–N1	2.212(2)	Zn1–S2	2.4516(7)
O1–C6	1.265(3)	Zn1–S4	2.4109(7)
S2–C11	1.626(3)	S2–C6	1.716(3)
S3–C12	1.624(3)	S4–C12	1.712(3)
N2–C4	1.285(3)	N2–C4	1.290(3)
N2–N3	1.389(3)	N2–N3	1.370(3)
N3–C6	1.317(3)	N6–N7	1.364(3)
N5–C11	1.146(3)	N3–C6	1.327(3)
N6–C12	1.149(4)	N4–C6	1.360(3)
		N6–C10	1.301(3)
		N7–C12	1.332(3)
		N8–C12	1.360(3)
N6–Zn1–N5	110.73(11)	N2–Zn1–N6	166.84(8)
N6–Zn1–N2	121.74(10)	N2–Zn1–N5	103.08(7)
N5–Zn1–N2	127.42(10)	N6–Zn1–N5	75.28(7)
N6–Zn1–O1	96.93(10)	N2–Zn1–N1	73.63(8)
N5–Zn1–O1	97.85(9)	N6–Zn1–N1	93.21(8)
N2–Zn1–O1	74.02(8)	N5–Zn1–N1	84.54(8)
N6–Zn1–N1	101.94(10)	N2–Zn1–S4	101.19(5)
N5–Zn1–N1	97.92(9)	N6–Zn1–S4	79.42(5)
N2–Zn1–N1	75.37(8)	N5–Zn1–S4	154.65(6)
O1–Zn1–N1	149.20(7)	N1–Zn1–S4	95.42(6)
C6–O1–Zn1	109.97(16)	N2–Zn1–S2	79.08(6)
C11–N5–Zn1	168.5(3)	N6–Zn1–S2	113.88(6)
C12–N6–Zn1	171.7(2)	N5–Zn1–S2	91.66(6)
N5–C11–S2	179.0(3)	N1–Zn1–S2	150.76(6)
N6–C12–S3	179.2(3)	S4–Zn1–S2	100.03(3)
		C6–S2–Zn1	95.20(9)
		C12–S4–Zn1	95.96(8)

Table 2. Optimization of the reaction conditions.

Entry	Catalyst	Mol%	Temp.(°C)	Solvent	Additive (0.5 eq.)	% Isolated Yield [1]
1	**1**	10	120	toluene (1 M)	-	85
2	**HL¹Cl**	10	120	toluene (1 M)	-	0
3	**3**	10	120	toluene (1 M)	-	67
4	**HL³Cl**	10	120	toluene (1 M)	-	0
5	**2**	10	120	toluene (1 M)	-	56
6	**1**	5	110	neat	-	51
7	**1**	10	110	neat	-	65
8	**3**	10	110	neat	-	57
9	**1**	5	130	neat	MgSO$_4$	91
10	**3**	5	130	neat	MgSO$_4$	61
11 [2]	**1**	5	130	neat	MgSO$_4$	33

All reactions were performed on a 0.5 mmol scale and the reaction time was 16 h unless otherwise noted. [1] The progress of the reaction was monitored by gas chromatography/mass spectroscopy (GC/MS) analysis, using *n*-octane as the internal standard and the isolated yields reported correspond to the pure product after chromatographic purification. [2] The reaction was stopped after 3 h.

The molecular structure of **2** is shown in Figure 2. Selected bond distances and angles are given in Table 1. The neutral complex molecule [Zn(**L²**)$_2$] crystallizes in the monoclinic crystal system with space group *P*2$_1$/*c*. In complex **2**, two deprotonated ligand molecules **L²** coordinate

the Zn(II) ion in a meridional fashion, forming a distorted octahedral complex by chelation through two NNS donor atom sets. Each ligand coordinates to metallic center through thiazole nitrogen, imine nitrogen and thiolate sulfur atoms. The tridentate coordination of each ligand implies the formation of two fused five-membered chelate rings Zn–N–C–C–N and Zn–N–N–C–S. The chelate rings (Zn1–N5–C9–C10–N6 and Zn1–N6–N7–C12–S4) are nearly coplanar, while the other pair (Zn1–N1–C3–C4–N2 and Zn1–N2–N3–C6–S2) deviates significantly from coplanarity, as indicated by the dihedral angles of 2.2° and 7.1°, respectively. In addition, the two chelation planes comprising the atoms N–N–S–Zn are practically perpendicular (dihedral angle = 89.7°). The octahedral complex molecule of **2** is comparable with the Zn(II) complex containing a similar ligand (2-acetylthiazole (N4)-phenylthiosemicarbazone) (CSD refcode KUMPEP) [13], although the latter is much more distorted due to the presence of the phenyl group at the terminal nitrogen atom of the thiosemicarbazone ligand, as evidenced by the smaller dihedral angle between chelation planes (N–N–S–Zn) compared to that observed in **2** (83.9° vs. 89.7°). One of the measures of the octahedral strain is average ΔO_h value, defined as the mean deviation of 12 octahedral angles from ideal 90°. The complex **2** shows less octahedral strain in comparison to that observed in analogous Zn(II) complex with 2-acetylthiazole (N4)-phenylthiosemicarbazone. The calculated ΔO_h values are 10° for the former and 12° for the latter complex. The mean Zn–**L** bond lengths (Zn–$N_{1,3-thiazole}$ 2.2525 Å, Zn–$S_{thiolate}$ 2.4313 Å and Zn–N_{imine} 2.148 Å) observed in complex **2** are similar to those found in its structural analogue (Zn–$N_{1,3-thiazole}$ 2.2310 Å, Zn–$S_{thiolate}$ 2.4331 and Zn–N_{imine} 2.1877Å).
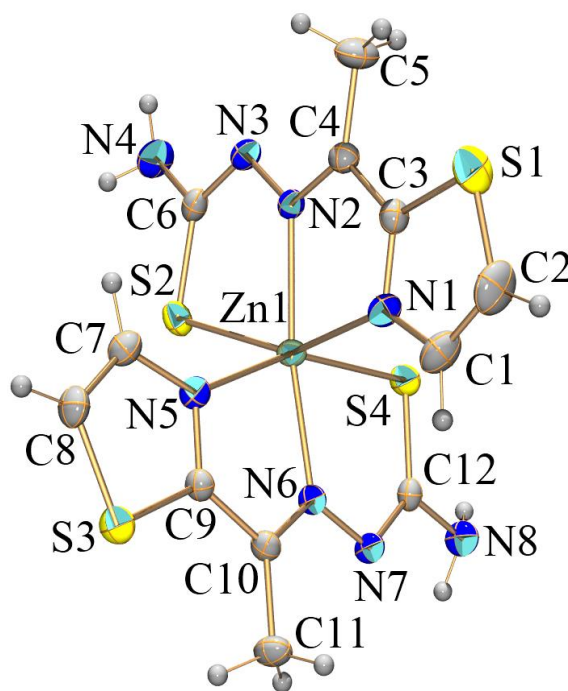

Figure 2. ORTEP presentation of the molecular structure of [Zn(**L**^{2})$_2$] (**2**). Thermal ellipsoids are drawn at the 30% probability level.

In the crystals of complex **2**, molecules self-assemble within the layer parallel with the (1 0 0) lattice plain by means of intermolecular hydrogen bonds between terminal NH_2 groups (N4 and N8) serving as hydrogen bond donors and thiolate sulfur atoms S4 at $1 - x$, $-1/2 + y$, $\frac{1}{2} - z$ and S2 at $1 - x$, $2 - y$, $-z$ serving as acceptors (Table S3, Figure S2a in the Supplementary Materials). The complex molecules belonging to neighboring layers are linked through weak $\pi\cdots\pi$ interactions involving heteroaromatic 1,3-thiazole rings to form a 3D supramolecular structure (Table S4 and Figure S2b in the Supplementary Materials). In addition, the molecules of **2** are linked along *a* crystallographic axis by weak $C_{aromatic}$–H$\cdots N_{hydrazone}$ contacts.

2.3. Evaluation of the Zinc Complexes' Catalytic Activity in the KA^2 Coupling Reaction

We chose cyclohexanone, pyrrolidine and phenylacetylene as a model substrate triad. A promising result was obtained when complex **1** was used in 10 mol% loading in toluene, affording the product in 85% isolated yield after 16 h (Entry 1, Table 2). As expected, when ligand **HL^1**Cl was used as a possible catalyst in a control experiment, the desired propargylamine was not formed. Complex **3** led to a 67% yield under the same conditions, while complex **2** also displayed moderate catalytic activity (Entries 3 and 5, Table 2), suggesting that the zinc center is no longer fully coordinated under the reaction conditions. Removing the solvent while reducing the temperature and catalyst loading also led to moderate yields in the cases of both **1** and **3** (Entries 6–8, Table 2), while using MgSO$_4$ as a water-scavenging additive, in combination with an increase in temperature, led to the highest yield, when complex **1** was used in 5 mol% loading (Entry 9, Table 2). Under the same conditions, complex **3** led to moderate yield, while reducing the reaction time to 3 h led to incomplete conversion and low yield (Entries 10 and 11 respectively, Table 2), suggesting that the reaction conditions outlined in entry 9 of Table 2 were optimal. Of note, when taking into account the reactivity of simple zinc salts, complex **1** performs comparably well in this reaction. However, lower catalyst loading is required under the conditions described herein, while, in the case of zinc acetate, 10 mol% was essential in order to reach yields above 90%, in combination with dry/inert conditions.

Several substrate combinations were coupled under the aforementioned conditions, as shown in Scheme 2. Piperidine led to compound **4b** in high yield, as was the case in the parent, Zn-based, ligand-free system and the more recently reported Mn-based system [34,42]. Propargylamine **4c** was obtained in moderate yield, while using a linear ketone in combination with pyrrolidine afforded compound **4d** in 72% yield. Propargylamine **4e**, bearing an ester moiety that can be used for further functionalization, was synthesized in good yield, while the primary amine-derived compound **4f** was also successfully synthesized, albeit in moderate yield because of the stability of the intermediate imine. When the steric bulk of the linear ketone was increased, the yield dropped significantly, highlighting the crucial effect of steric hindrance in the outcome of this reaction (compound **4g**). When an aliphatic alkyne was used in combination with *N*-phenylpiperazine, propargylamine **4h** was obtained in 37% isolated yield. In order to assess the effect of a less functionalized aliphatic alkyne, 1-octyne was used and compound **4i** was isolated in 70% yield. Finally, cyclopentanone was chosen as a coupling partner and, as anticipated based on known reactivity trends, compound **4j** was obtained in moderate yield [34,42]. Overall, complex **1** allows for lower catalyst loading when compared to simple zinc salts and is more robust under harsh, ambient conditions [34]; however, the limitations of this coupling reaction and the generally observed trends regarding substrate scope persist in this case as well.

2.4. Density Functional Theory (DFT) Optimized Structures and Highest Occupied Molecular Orbital-Lowest Unoccupied Molecular Orbital (HOMO-LUMO) Analysis

In order to calculate the ground-state geometries of the complexes, DFT calculations of [ZnL^1(NCS)$_2$] (**1**) and [Zn(L^2)$_2$] (**2**), as well as [ZnL^3(NCS)$_2$] (**3**) complexes have been performed, as described below. DFT calculations predict five-fold coordination for both [ZnL^1(NCS)$_2$] and [ZnL^3(NCS)$_2$] complexes with tridentate ligands **HL^1**Cl and **HL^3**Cl and two nitrogen atoms from thiocyanate ligands (Figure 3), thereby supporting the experimental X-ray diffraction (XRD) results. In complex **2** DFT results show that two tridentate ligand molecules **L^2** coordinate the Zn(II) ion through thiazole nitrogen, imine nitrogen and thiolate sulfur atoms, forming an octahedral complex with four fused five-membered chelate rings, in agreement with experimental data. Selected bond lengths and values of valence angles are summarized in Table S5. The calculated geometric parameters of mixed ligand complexes are compared with the X-ray diffraction structures and show good agreement.
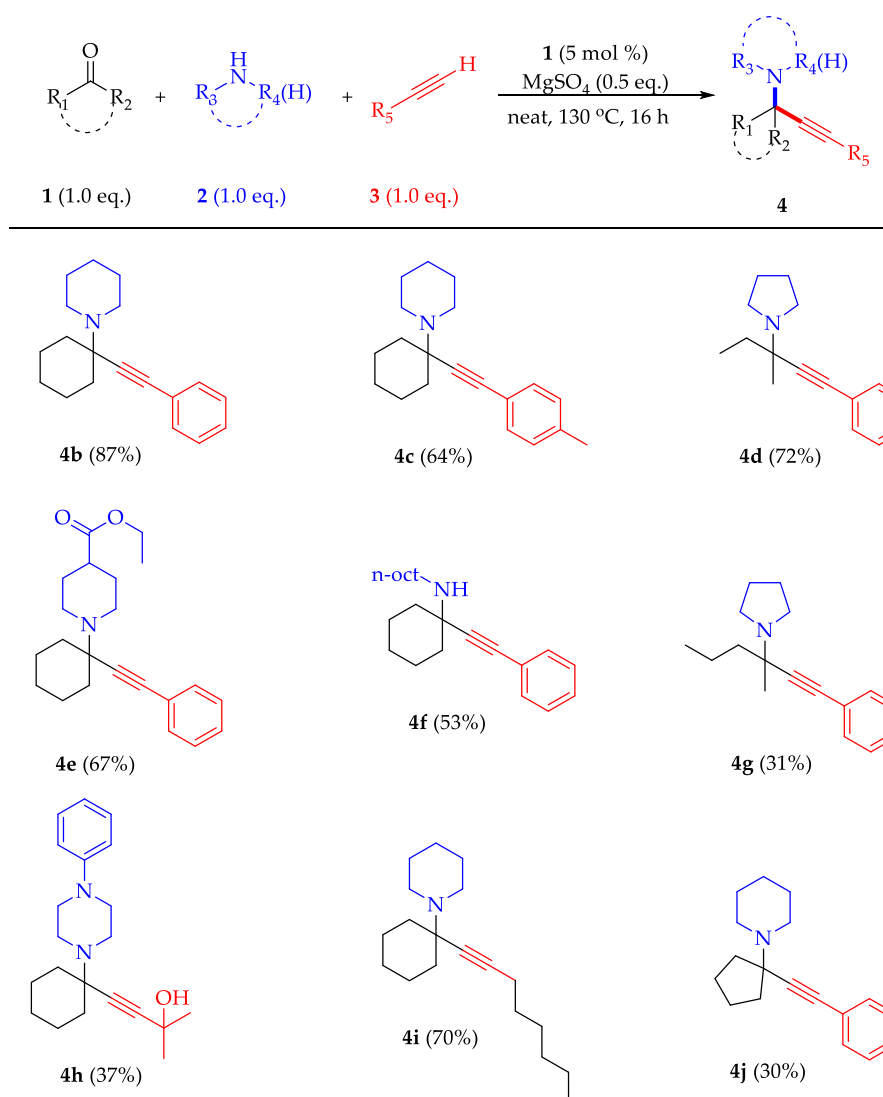
Scheme 2. Substrate scope of the reaction system under the optimal conditions. All reactions were performed on a 0.5 mmol scale and isolated yields after column chromatography are shown in parentheses.
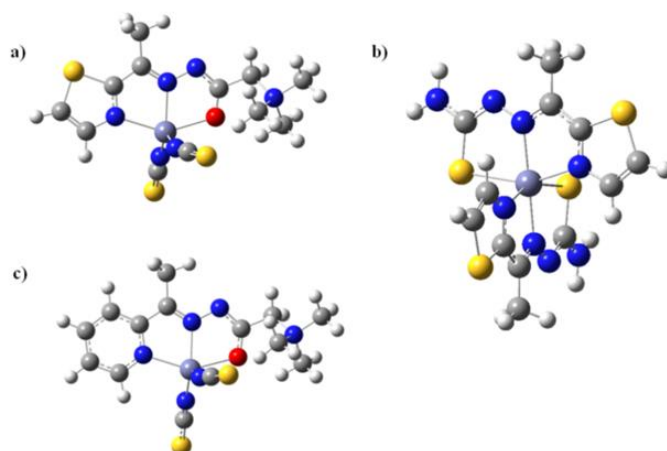

Figure 3. Density functional theory (DFT) optimized geometries of: (**a**) [ZnL^1(NCS)$_2$] (**1**); (**b**) [Zn(L^2)$_2$] (**2**); and (**c**) [ZnL^3(NCS)$_2$] (**3**).

The HOMO-LUMO energies of the complexes provide information about energetic behavior and stability of the complexes. The energy gap between HOMO and LUMO, determines reactivity and kinetic stability of molecules [43–45]. The chemical hardness (η) is a good indicator of the chemical stability. The molecules having a large energy gap are known as hard and having a small energy gap are known as soft molecules. The soft molecules are more polarizable than the hard ones because they need little energy for excitation [46,47]. The chemical potential (μ), hardness value (η), softness (S), electronegativity (χ) and electrophilicity index (ω) of molecules are formulated by the equations [47]:

$$\mu = -(-E_{HOMO} - E_{LUMO})/2, \tag{1}$$

$$\eta = (-E_{HOMO} + E_{LUMO})/2, \tag{2}$$

$$S = 1/2\eta, \tag{3}$$

$$\chi = (-E_{HOMO} - E_{LUMO})/2, \tag{4}$$

$$\omega = \mu^2/2\eta, \tag{5}$$

where E_{HOMO} and E_{LUMO} are the energies of the HOMO and LUMO orbitals. The negative chemical potential indicates complex to be stable in such a way that does not decompose spontaneously into its elements. Hardness measures the resistance to change in the electron distribution in a molecule.

The HOMO-LUMO energy calculations were performed within the time-dependent density functional theory (TD-DFT) approach at the B3LYP/6-31G level of theory in vacuum and toluene. This functional has been employed with a great success in reactivity studies, with a good compromise between accuracy and computational cost [48]. To examine the basis set dependence of the DFT HOMO and LUMO energies, we also performed TD-DFT calculations on the investigated systems using the B3LYP functional with a larger basis set such as 6-311G(d,p). Results are presented in the Table S6. We obtained small differences between the HOMO and LUMO energies calculated at B3LYP level of theory by using the 6-31G and 6-311G(d,p) basis sets, ranging from 0.07 to 0.22eV. It has been already found that HOMO energies, negative values of LUMO energies and TD-DFT HOMO-LUMO gaps are generally less sensitive to the basis set [49].

The HOMO and LUMO and their energies were calculated to locate the high- and low-density regions in all complexes and are shown in Figure 4. The HOMOs of [ZnL^1(NCS)$_2$] (**1**) and [ZnL^3(NCS)$_2$] (**3**) complexes are delocalized mainly at the linear monodentate ligands NCS$^-$ and metal centers, whereas the LUMOs are delocalized on the planar ring of Schiff base in equatorial plane (Figure 4). The HOMOs of the complex [Zn(L^2)$_2$] (**2**) are delocalized mainly at the five-membered heterocyclic rings with terminal NH$_2$ groups. The LUMOs of the complex [Zn(L^2)$_2$] (**2**) are delocalized at the five-membered heterocyclic chelate rings of the two tridentate ligands. The calculated values of reactivity descriptors of complexes are given in Table 3. The negative values of chemical potential (-3.886, -3.597 and -3.670 eV) show their stability suggesting that these do not undergo decomposition into their components. As shown in Table 3, the compound that has the lowest energy gap in comparison to the two other complexes is the compound **1** (ΔEgap is 2.167 eV in vacuum and 2.977 eV in toluene). This lower energy gap allows it to be the softest molecule. The magnitude of chemical hardness, supported by the HOMO–LUMO energy gap, for complexes **1**, **2** and **3** have been found to be: 1.083, 1.456, and 1.232 eV, respectively (Table 3). Chemical hardness (softness) value of complex **1** is lower (greater) among all the investigated complexes, both in the gas phase and toluene. Hence, complex **1** is found to be more reactive than all the compounds which is in agreement with experimental catalytic data. The compound that has the lowest LUMO energy is the compound 1 ($E = -2.803$ eV) which signifies that it can be the best electron acceptor [50]. Besides, the electrophilicity index values ω given in Table 3 for complexes (6.971, 4.443 and 5.466 eV, respectively) related to chemical potential and hardness indicate that compound **1** is the strongest electrophile among all compounds. Compound **1** possesses a higher electronegativity value ($\chi = 3.886$ eV) than all compounds, a characteristic that could explain its superior activity in catalysis, when compared to the other complexes evaluated herein [34].

Results were confirmed by using another DFT model denoted as BVP86/6-311G(d,p) with the lowest HOMO-LUMO energy gap for complex **1**. The differences between TD-DFT gaps calculated with selected different functionals are small. For instance, B3LYP and BVP86 predict relatively good HOMO and LUMO energies for investigated complexes with errors ranging from 0.56 to 0.73 eV.
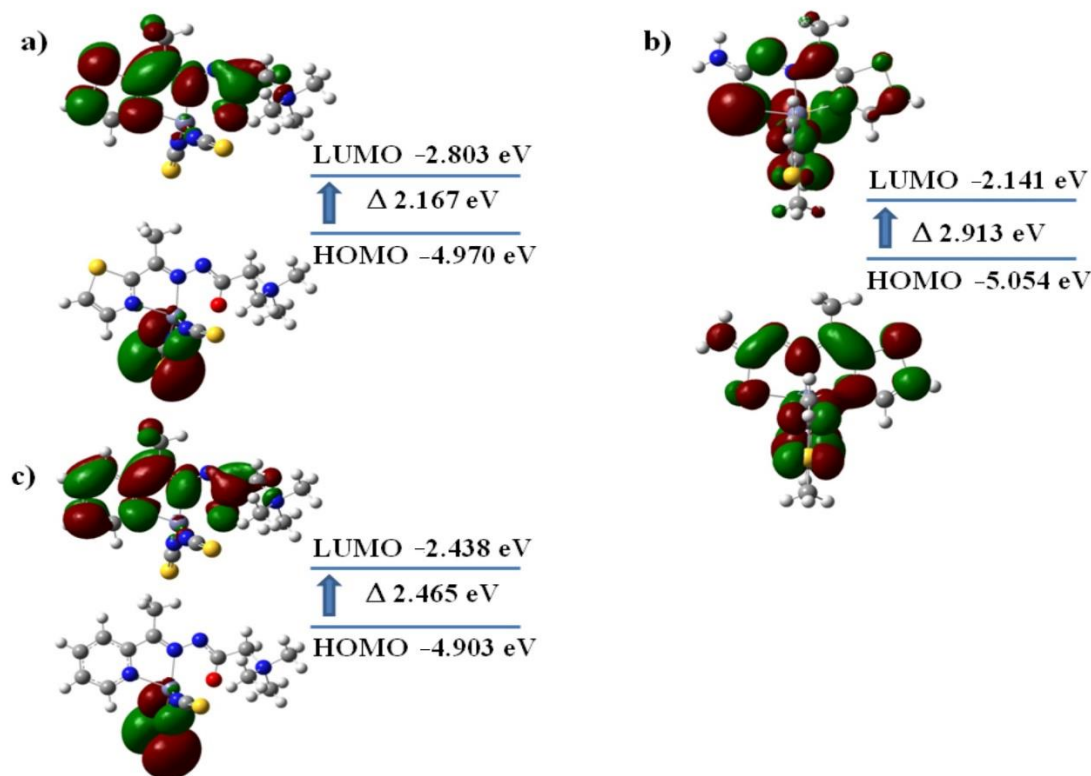

Figure 4. Molecular orbital plots and energy levels of the highest occupied molecular orbital (HOMO), the lowest unoccupied molecular orbital (LUMO) and HOMO-LUMO transitions of: (**a**) [Zn**L**^{1}(NCS)$_2$] (**1**); (**b**) [Zn(**L**^{2})$_2$] (**2**); and (**c**) [Zn**L**^{3}(NCS)$_2$] (**3**).

Table 3. Quantum chemical descriptors for complexes in vacuum and toluene (in brackets).

	[Zn**L**^{1}(NCS)$_2$] (1)	[Zn(**L**^{2})$_2$] (2)	[Zn**L**^{3}(NCS)$_2$] (3)
E_{HOMO} (eV)	−4.970 (−5.692)	−5.054 (−5.268)	−4.903 (−5.645)
E_{LUMO} (eV)	−2.803 (−2.695)	−2.141 (−2.252)	−2.438 (−2.330)
ΔE_{gap} (eV)	2.167 (2.977)	2.913 (3.016)	2.465 (3.315)
μ (eV)	−3.886 (−4.193)	−3.597 (−3.76)	−3.670 (−3.987)
η (eV)	1.083 (1.488)	1.456 (1.508)	1.232 (1.657)
S (eV)	0.461 (0.336)	0.343 (0.331)	0.405 (0.301)
X (eV)	3.886 (4.193)	3.597 (3.760)	3.670 (3.987)
ω (eV)	6.971 (5.908)	4.443 (4.687)	5.466 (4.797)

3. Materials and Methods

2-Acetylpyridine (≥99%), 2-acetylthiazole (99%), thiosemicarbazide (99%) and Girard's T reagent (99%) were obtained from Aldrich. IR spectra were recorded on a Nicolet 6700 Fourier transform infrared (FT-IR) spectrometer using the attenuated total reflectance (ATR) technique in the region 4000−400 cm^{-1} (vs-very strong, s-strong, m-medium, w-weak, bs-broad signal). ^{1}H- and ^{13}C-NMR spectra were recorded on a Bruker Avance Ultrashield 500 plus spectrometer (^{1}H at 500 MHz; ^{13}C at 125 MHz) at room temperature using TMS as internal standard in DMSO-d_6, or on a Varian Mercury 200 MHz spectrometer (^{1}H at 200 MHz; ^{13}C at 50 MHz) or a Brucker Avance 400 MHz instrument (^{1}H at 400 MHz; ^{13}C at 101 MHz) using CDCl$_3$ as the solvent. Chemical shifts are expressed in ppm

(δ) values and coupling constants (*J*) in Hz. Elemental analyses (C, H, N and S) were performed by standard micro-methods using the ELEMENTARVario ELIII C.H.N.S.O analyzer. Molar conductivities were measured at room temperature (25 °C) on a digital conductivity-meter JENWAY-4009. GC/MS spectra were recorded with a Shimandzu R GCMS-QP2010 Plus Chromatograph Mass Spectrometer using a MEGAR (MEGA-5, F.T: 0.25 μm, I.D.: 0.25 mm, L: 30 m, Tmax: 350 °C, Column ID# 11475) column, using n-octane as the internal standard.

3.1. Synthesis of (E)-N,N,N-trimethyl-2-oxo-2-(2-(1-(thiazol-2-yl)ethylidene)hydrazinyl)ethan-1-aminium Chloride (**HL^{1}Cl**)

The ligand **HL^{1}Cl** was synthesized by the reaction of Girard's reagent T (1.676 g, 10 mmol) and 2-acetylthiazole (1036 μL, 10 mmol) in water (20 mL). Reaction mixture was acidified with 3–4 drops of 2 M HCl and refluxed for 3 h. After cooling to the room temperature, white precipitate was filtered and washed with water. Yield: 2.54 g (92%). Anal. Calcd. (%) for $C_{10}H_{17}N_4OSCl$: C, 43.40; H, 6.19; N, 20.24; S, 11.58. Found (%): C, 43.45; H, 6.21; N, 20.20; S, 11.52. IR (ATR, cm^{-1}): 3387w, 3129w, 3092m, 3018m, 2955s, 1702vs, 1612w, 1550vs, 1487s, 1401m, 1300w, 1201s, 1135w, 976w, 945w, 914m, 787w, 748w, 684w, 585w, 552w. ^{1}H-NMR (500 MHz, DMSO-d_6), δ (ppm): 2.41, (s, 3H, C5-H); 2.53, (s, 3H, C5-H); 3.30, (s, 9H, C8-H); 3.34, (s, 9H, C8-H); 4.60, (s, 2H, C7-H); 4.82, (s, 2H, C7-H); 7.848, (d, 1H, $J_{C2-H/C3-H}$ = 5 Hz, C2-H); 7.854, (d, 1H, $J_{C2-H/C3-H}$ = 5 Hz, C2-H); 7.926, (d, 1H, $J_{C2-H/C3-H}$ = 5 Hz, C3-H); 7.932, (d, 1H, $J_{C2-H/C3-H}$ = 5 Hz, C3-H); 11.61, (s, 1H, N-H); 11.86, (s, 1H, N-H). ^{13}C-NMR (125 MHz, DMSO-d_6), δ (ppm): 13.9, (C5); 15.05, (C5); 53.6, (C8); 53.9, (C8); 63.0, (C7); 63.8, (C7); 123.3, (C2); 123.6, (C2); 143.9, (C3); 144.00, (C3); 147.00, (C4); 150.8, (C4); 161.2, (C1); 166. 8, (C1); 167.0, (C6); 167.3, (C6).

3.2. Synthesis of [ZnL^1(NCS)$_2$]·2H$_2$O (**1**)

The Zn(II) complex **1** was synthesized by the reaction of Zn(OAc)$_2$·2H$_2$O (75 mg, 0.30 mmol), ligand **HL^{1}Cl** (83 mg, 0.30 mmol) and NH$_4$SCN (60 mg, 0.78 mmol) in a solvent mixture of water/methanol (10/10 mL). The solution was refluxed for 4 h. After refrigeration of the reaction solution at −8 °C for two weeks pale yellow crystals suitable for X-ray analysis were formed. Yield: 0.11 g (83%). Anal. Calcd. (%) for $C_{12}H_{20}N_6O_3S_3Zn$: C, 36.71; H, 5.13; N, 21.41; S, 24.51. Found (%): C, 36.55; H, 5.15; N, 21.27; S, 24.31. IR (ATR, cm^{-1}): 3502s, 3383s, 3123m, 3055w, 2959w, 2088vs, 1610s, 1536s, 1475s, 1424s, 1402s, 1341m, 1290w, 1237w, 1151w, 1095w, 1064w, 1012w, 988w, 923w, 880w, 746w, 556w. ^{1}H-NMR (500 MHz, DMSO-d_6), δ (ppm): 2.54, (s, 3H, C5-H); 3.27, (s, 9H, C8-H); 4.20, (s, 2H, C7-H); 8.06, (d, 1H, $J_{C2-H/C3-H}$ = 2.2 Hz, C2-H); 8.16, (d, 1H, $J_{C2-H/C3-H}$ = 2.2 Hz, C3-H). ^{13}C-NMR (125 MHz, DMSO-d_6), δ (ppm): 15.4, (C5); 53.8, (C8); 66.7, (C7); 125.7, (C3); 134.3, (C9); 142.5, (C2); 147.3, (C4); 166.2, (C1); 171.7, (C6).

3.3. Synthesis of Ligand **HL^2** (E)-2-(1-(thiazol-2-yl)ethylidene)hydrazine-1-carbothioamide

The ligand **HL^2** was synthesized by the reaction of thiosemicarbazide and 2-acetylthiazole in water according to the previously described method [12]. Yield 1.82 g (91%). IR (ATR, cm^{-1}): 3436s, 3248s, 3188s, 3099m, 3071m, 2983m, 2066w, 1648w, 1589s, 1510s, 1482s, 1452m, 1425s, 1365m, 1282m, 1166m, 1107m, 1069m, 1039m, 958w, 881w, 847w, 755w, 712w, 638w. Anal. Calcd. (%) for $C_6H_8N_4S_2$: C, 35.98; H, 4.03; N, 27.98; S, 32.02. Found (%): C, 35.74; H, 4.26; N, 27.88; S, 31.98. ^{1}H-NMR (500 MHz, DMSO-d_6), δ (ppm): 7.89, (C4-H, d J^3 = 5 Hz); 7.80, (C5-H, d, J^3 = 5 Hz); 2.43, (C7-H$_3$, s); 10.67, (N-H, s); 8.53 and 7.69, (N-H$_2$, bs). ^{13}C-NMR (125 MHz, DMSO-d_6), δ (ppm): 14.1, (C7); 144.7, (C2); 179.4, (C8); 167.5, (C6); 143.7, (C4); 123.1, (C5).

3.4. Synthesis of [Zn(L^2)$_2$] (**2**)

The Zn(II) complex **2** was synthesized by the reaction of Zn(BF$_4$)$_2$·6H$_2$O (72 mg, 0.20 mmol), ligand **HL^{2}Cl** (40 mg, 0.20 mmol) and NaN$_3$ (30 mg, 0.46mmol) in solvent mixture of acetonitrile/water (15/5 mL). The solution was refluxed for 4 h. After refrigeration of the reaction solution at −8 °C for one-week yellow crystals suitable for X-ray analysis were formed. Yield: 0.08 g (87%). Anal. Calcd.

(%) for $C_{12}H_{14}N_8S_4Zn$: C, 36.16; H, 3.54; N, 28.12; S, 32.18. Found (%): C, 36.04; H, 3.56; N, 28.02; S, 32.07. IR (ATR, cm^{-1}): 3571w, 3496w, 3436m, 3308vs, 3169s, 3109s, 2925w, 2255w, 2185w, 2078m, 1632m, 1589m, 1569m, 1496s, 1425vs, 1375vs, 1298s, 1198vs, 1162s, 1097s, 1029m, 882w, 783m, 726w, 677m, 644w, 596w, 547w, 480w. ^{1}H-NMR (500 MHz, DMSO-d_6), δ (ppm): 2.43, (s, 3H, C5-H); 7.45, (s, 2H, NH2); 7.88, (d, 1H, C2-H); 7.94, (d, 1H, C6-H). ^{13}C-NMR (125 MHz, DMSO-d_6), δ (ppm): 15.9, (C5); 122.5, (C3); 139.2, (C4); 142.4, (C2); 167.3, (C1); 181.7, (C6).

3.5. Synthesis of Ligand HL^{3}Cl (E)-N,N,N-trimethyl-2-oxo-2-(2-(1-(pyridin-2-yl)ethylidene)hydrazinyl) ethan-1-aminium Chloride

The **HL^{3}Cl** ligand was synthesized by the reaction of 2-acetylpyridine and Girard's T reagent according to the previously described method [8]. Yield 2.36 g (87%). IR (ATR, cm^{-1}): 3387w, 3127m, 3090m, 3049m, 3016m, 2950s, 1700vs, 1612w, 1549s, 1485m, 1400m, 1300w, 1253w, 1200s, 1153w, 1135m, 1095w, 1073m, 975w, 944w, 914m, 748w, 683w.

3.6. Synthesis of [ZnL^3(NCS)$_2$]·0.5CH$_3$OH Complex (3)

The Zn(II) complex **3** was synthesized by the reaction of ligand **HL^{3}Cl**, Zn(OAc)$_2$·2H$_2$O and NH$_4$SCN according to the previously described method [8]. Yield 0.08 g (94%). IR (ATR, cm^{-1}): 3030w, 2067vs, 1639w, 1620w, 1592w, 1566m, 1535s, 1464m, 1437m, 1397m, 1366m, 1339m, 1302m, 1200w, 1145w, 1074m, 1019m, 975w, 914w, 782w, 749 (w). $\lambda_M = 28\ \Omega^{-1}cm^2mol^{-1}$.

3.7. X-Ray Crystallography

The molecular structures of complexes **1** and **2** were determined by single-crystal X-ray diffraction. Crystallographic data and refinement details are given in Table S7. The X-ray intensity data for **1** were collected at room temperature on a Nonius Kappa CCD diffractometer equipped with graphite-monochromator utilizing MoKα radiation (λ = 0.71073 Å). Data reduction and cell refinement was carried out using DENZO and SCALPACK [51]. Diffraction data for **2** were collected at room temperature with an Agilent SuperNova dual source diffractometer using an Atlas detector and equipped with mirror-monochromated MoKα radiation (λ = 0.71073 Å). The data were processed by using CrysAlis PRO [52]. All the structures were solved using SIR-92 [53] and refined against F^2 on all data by full-matrix least-squares with SHELXL–2014 [54]. All non-hydrogen atoms were refined anisotropically. The water bonded hydrogen atoms in **1** was located in a difference map and refined with the distance restraints (DFIX) with O–H = 0.96 Å and with U_{iso}(H) = 1.5U_{eq}(O). All other hydrogen atoms were included in the model at geometrically calculated positions and refined using a riding model. Crystallographic data for the structures reported in this paper have been deposited with the CCDC 2021000 (for **1**) and 2021001 (for **2**). CCDC 2021000 and 2021001 contain the supplementary crystallographic data for this paper. These data can be obtained free of charge via http://www.ccdc.cam.ac.uk/conts/retrieving.html (or from the CCDC, 12 Union Road, Cambridge CB2 1EZ, UK; Fax: +44 1223 336033; E-mail: deposit@ccdc.cam.ac.uk).

3.8. Catalysis General Procedure

A Teflon sealed screw-cap pressure tube equipped with a stirring bar and a rubber septum or a screw-cap vial, was charged with x mol% of the catalyst and 0.5 eq. of the additive (MgSO$_4$) unless otherwise noted. Under air, 0.5 mmol of the amine were added and the mixture was stirred until the solid was partially dissolved. 0.5 mmol of the alkyne were added and the mixture was stirred at room temperature. Finally, 0.5 mmol of the ketone were added and the reaction was allowed to stir in a preheated oil bath, for the appropriate time. After cooling to room temperature, ethyl acetate was added (2 × 5 mL) and the mixture was stirred for 5 min. The mixture was filtered through a short silica gel plug, in order to remove inorganic impurities, concentrated under vacuum and loaded atop a silica gel column. Gradient column chromatography with ethyl acetate/petroleum ether furnished the desired products. All products were characterized by ^{1}H-NMR, and ^{13}C{^{1}H}-NMR which were all in

agreement with the assigned structures and the data reported in the literature ([34,42] and references cited therein]).

Characterization Data for the Synthesized Propargylamines

1-(1-(Phenylethynyl)cyclohexyl)pyrrolidine (**4a**): Obtained as an orange/yellow oil in 91% yield (115 mg, 0.46 mmol). ^{1}H-NMR (200 MHz, CDCl$_3$) δ 7.44 (dd, *J* = 6.7, 3.1 Hz, 2H), 7.30 (m, 3H), 2.82 (t, *J* = 5.9 Hz, 4H), 2.13–1.94 (m, 2H), 1.91–1.41 (m, 12H, overlapping peaks). ^{13}C{^{1}H}-NMR (50 MHz, CDCl$_3$) δ 131.7, 128.1, 127.6, 123.6, 90.3, 86.1, 59.3, 47.0, 37.8, 25.7, 23.5, 23.0.

1-(1-(Phenylethynyl)cyclohexyl)piperidine (**4b**): Obtained as a yellow oil in 87% yield (116 mg, 0.44 mmol). ^{1}H-NMR (400 MHz, CDCl$_3$) δ 7.47–7.36 (m, 2H), 7.28–7.23 (m, 3H), 2.70 (m, 4H), 2.11–2.05 (m, 2H), 1.83–1.34 (m, 14H, overlapping peaks). ^{13}C{^{1}H}-NMR (101 MHz, CDCl$_3$) δ 131.9, 128.4, 127.8, 124.0, 90.6, 86.3, 59.7, 47.3, 35.8, 26.6, 25.8, 24.9, 23.2.

1-(1-(p-Tolylethynyl)cyclohexyl)piperidine (**4c**): Obtained as a yellow oil in 64% yield (91 mg, 0.32 mmol). ^{1}H-NMR (400 MHz, CDCl$_3$) δ 7.33 (d, *J* = 7.9 Hz, 2H), 7.10 (d, *J* = 7.9 Hz, 2H), 2.73 (s, 4H), 2.34 (s, 3H), 2.12–2.09 (m, 2H), 1.78–1.42 (m, 14H, overlapping peaks). ^{13}C{^{1}H}-NMR (101 MHz, CDCl$_3$) δ 137.9, 131.7, 129.1, 120.6, 90.4, 86.7, 59.9, 47.3, 35.7, 26.4, 25.8, 24.7, 23.3, 21.5.

1-(3-Methyl-1-phenylpent-1-yn-3-yl)pyrrolidine (**4d**): Obtained as an orange/brown oil in 72% yield (82 mg, 0.36 mmol). ^{1}H-NMR (400 MHz, CDCl$_3$) δ 7.45–7.38 (m, 2H), 7.32–7.26 (m, 3H), 2.80 (t, *J* = 5.8 Hz, 4H), 1.84–1.79 (m, 4H), 1.74–1.65 (m, 2H), 1.42 (s, 3H), 1.05 (t, *J* = 7.5 Hz, 3H). ^{13}C{^{1}H}-NMR (101 MHz, CDCl$_3$) δ 131.7, 128.2, 127.7, 123.5, 90.9, 84.7, 58.6, 47.8, 33.9, 25.1, 23.7, 8.9.

1-(1-(Phenylethynyl)cyclohexyl)piperidine-4-carboxylate (**4e**): Obtained as a yellow oil in 67% yield (114 mg, 0.34 mmol). ^{1}H-NMR (200 MHz, CDCl$_3$) δ 7.42 (dd, *J* = 6.7, 3.0 Hz, 2H), 7.35–7.23 (m, 3H), 4.13 (q, *J* = 7.1 Hz, 2H), 3.15 (d, *J* = 11.6 Hz, 2H), 2.42–2.18 (t, *J* = 11.0 Hz, 3H), 2.13–1.43 (m, 14H), 1.24 (t, *J* = 7.1 Hz, 3H). ^{13}C{^{1}H}-NMR (50 MHz, CDCl$_3$) δ 175.4, 131.7, 128.3, 127.8, 123.6, 90.4, 86.2, 60.3, 59.0, 45.8, 41.6, 35.9, 28.9, 25.8, 22.9, 14.3.

N-Octyl-1-(phenylethynyl)cyclohexanamine (**4f**): Obtained as a yellow oil in 53% yield (83 mg, 0.27 mmol). ^{1}H-NMR (200 MHz, CDCl$_3$) δ 7.42 (dd, *J* = 6.7, 3.1 Hz, 2H), 7.33–7.23 (m, 3H), 2.79 (t, *J* = 7.1 Hz, 2H), 1.94 (d, *J* = 11.6 Hz, 2H), 1.74–1.07 (m, 20H), 0.88 (m, 3H). ^{13}C{^{1}H}-NMR (50 MHz, CDCl$_3$) δ 131.6, 128.1, 127.7, 123.6, 93.3, 84.6, 55.2, 43.2, 38.1, 31.8, 30.5, 29.5, 29.3, 27.5, 25.9, 23.1, 22.7, 14.1.

1-(3-Methyl-1-phenylhex-1-yn-3-yl)pyrrolidine (**4g**): Prepared according to the general procedure and obtained as an orange/brown oil in 31% yield (37 mg, 0.16 mmol). ^{1}H-NMR (200 MHz, CDCl$_3$) δ 7.45–7.36 (m, 2H), 7.28–7.25 (m, 3H), 2.79 (t, *J* = 5.4 Hz, 4H), 1.85–1.74 (m, 4H), 1.73–1.47 (m, 4H), 1.43 (s, 3H), 0.95 (t, *J* = 7.1 Hz, 3H). ^{13}C{^{1}H}-NMR (50 MHz, CDCl$_3$) δ 132.0, 128.4, 127.9, 123.8, 91.5, 84.7, 58.3, 48.0, 44.0, 26.1, 23.9, 18.0, 14.8.

2-Methyl-4-(1-(4-phenylpiperazin-1-yl)cyclohexyl)but-3-yn-2-ol (**4h**): Obtained as an orange solid in 37% yield (60 mg, 0.19 mmol). ^{1}H-NMR (400 MHz, CDCl$_3$) δ 7.26 (m, 2H), 6.93 (d, *J* = 8.6 Hz, 2H), 6.89–6.80 (m, 1H), 3.31–3.15 (m, 4H), 2.88–2.73 (m, 4H), 2.25 (br. s, 1H), 2.04–1.38 (m, 16H). ^{13}C{^{1}H}-NMR (50 MHz, CDCl$_3$) δ 151.3, 129.2, 119.7, 116.0, 91.6, 81.9, 65.4, 58.2, 49.6, 46.1, 35.7, 32.1, 25.7, 22.9.

1-(1-(Oct-1-yn-1-yl)cyclohexyl)piperidine (**4i**): Prepared according to the general procedure and obtained as a yellow oil in 70% yield (96 mg, 0.35 mmol). ^{1}H-NMR (400 MHz, CDCl$_3$) δ 2.70–2.50 (m, 4H), 2.22 (t, *J* = 6.7 Hz, 2H), 1.93 (d, *J* = 11.2 Hz, 2H), 1.78–1.70–1.24 (m, 22H), 0.95–0.79 (m, 3H). ^{13}C-NMR (101 MHz, CDCl$_3$) δ 85.8, 80.7, 58.9, 47.0, 36.0, 31.4, 29.3, 29.3, 25.9, 24.9, 23.2, 22.7, 18.7, 14.1.

1-(1-(Phenylethynyl)cyclopentyl)piperidine (**4j**): Prepared according to the general procedure and obtained as a yellow oil in 67% yield (339 mg, 1.34 mmol). ^{1}H-NMR (400 MHz, CDCl$_3$) δ 7.41 (dd, *J* = 6.5, 3.2 Hz, 2H), 7.31–7.25 (m, 3H), 2.75–2.60 (m, 4H), 2.15–2.10 (m, 2H), 1.87–1.44 (m, 12H, overlapping peaks). ^{13}C{^{1}H}-NMR (101 MHz, CDCl$_3$) δ 131.8, 128.3, 127.7, 123.9, 91.6, 85.4, 67.7, 50.4, 39.9, 26.3, 24.5, 23.5.

3.9. DFT Calculations

Density functional theory was used to determine the optimized geometries of complexes [Zn**L^1**(NCS)$_2$] (**1**) and [Zn(**L^2**)$_2$] (**2**). For comparison reasons the same calculations have been performed for [Zn**L^3**(NCS)$_2$] (**3**) complex [8]. All the DFT calculations were performed in gas phase with the Gaussian 09 [55] program at B3LYP/6–31G level [56–59] of theory. In order to evaluate the energetic behavior of complexes, the HOMO-LUMO energy calculations were performed within the TD-DFT approach using B3LYP/6-31G, B3LYP/6-311G (d,p) and BVP86/6-311G(d,p) methods in vacuum. In addition, HOMO-LUMO energy investigations were also conducted in toluene by using TD-DFT/PCM (polarizable continuum model) [60] calculations at B3LYP/6-31G level of theory. Calculations were carried on the PARADOX supercomputing facility [61].

4. Conclusions

In the reactions of Zn(II) with (*E*)-*N,N,N*-trimethyl-2-oxo-2-(2-(1-(thiazol-2-yl)ethylidene)hydrazinyl)ethan-1-aminium chloride (**HL^{1}Cl**) and (*E*)-2-(1-(thiazol-2-yl)ethylidene)hydrazine-1-carbothioamide (**HL^2**) in the presence of NH$_4$SCN and NaN$_3$, respectively, two different structural types of Zn(II) complexes were obtained and characterized by spectroscopic methods (IR and NMR) and single crystal X-ray diffraction methods. In **1** the Zn(II) ion is pentacoordinated with tridentate ligand **L^1** and two thiocyanate anions forming a distorted square pyramidal structure. In **2** the Zn(II) ion is hexacoordinated with two **L^2** molecules forming a distorted octahedral structure.

The DFT calculations of newly synthesized **1** and **2** complexes, as well as [Zn**L^3**(NCS)$_2$] (**3**) complex have been carried out for their structural determination, HOMO, LUMO study and to calculate reactivity descriptors. The lower kinetic stability and higher reactivity of complex **1** compared to the other two complexes have been found from the lower HOMO–LUMO energy gap value, in agreement with experimental data. The electrophilicity index value *ω* (6.971 eV in gas phase and 5.908 eV in toluene) indicates that compound **1** is the strongest electrophile than all investigated compounds. In addition, compound **1** possesses higher electronegativity value (*χ* = 3.886 eV) than all compounds. Therefore, it is the best electron acceptor and that feature can plausibly explain its better performance as a Lewis acid catalyst in the ketone-amine-alkyne coupling.

Supplementary Materials: The following are available online: Figure S1: (a) A view of the crystal packing of **1** showing complex molecules connected by means of OW-H⋯O, C$_{Me}$-H⋯S and C$_{Me}$-H⋯OW hydrogen bonds (dashed blue lines) into layer parallel with the (0 0 1) lattice plain; (b) A side view of the layers parallel with the (0 0 1) lattice plain related by the centers of symmetry showing the function of O1W in joining the neighboring layers, Figure S2: (a) A view of the crystal packing of **2** showing complex molecules connected by means of N–H⋯S hydrogen bonds (dashed blue lines) into layer parallel with the (1 0 0) lattice plain; (b) A side view of the layers showing intermolecular π⋯π contacts involving 1,3-thiazole rings. Hydrogen atoms not involved in hydrogen bonding are omitted for clarity, Figure S3–S22: ^{1}H- and ^{13}C{^{1}H}-NMR spectra of the synthesized propargylamines, Table S1. Structural parameters correlating the geometry of five-coordinate [ZnLX$_2$] complexes (L = tridentate hydrazone-based ligand; X = pseudohalde, halide or DMSO), Table S2. Hydrogen-bond parameters for [Zn**L^1**(NCS)$_2$]·2H$_2$O (**1**), Table S3. Hydrogen-bond parameters for [Zn(**L^2**)$_2$] (**2**), Table S4. Intermolecular π⋯π interaction parameters for complex **2**, Table S5. DFT calculated and experimental average values of selected bond lengths (Å) and angles (°) for [Zn**L^1**(NCS)$_2$] (**1**), [Zn(**L^2**)$_2$] (**2**) and [Zn**L^3**(NCS)$_2$] (**3**), Table S6. E$_{HOMO}$, E$_{LUMO}$ and their energy gaps calculated by using TD-DFT in vacuum at different levels of theory. Table S7. Crystal data and structure refinement details for **1** and **2**.

Author Contributions: T.T.A., D.M., and B.Č. contributed towards the syntheses, crystallization and characterization of the ligand and complexes, as well as the interpretation of the relevant results. A.P. collected single-crystal X-ray crystallographic data, solved the structures and performed their refinement. D.R. wrote the relevant XRD part of the paper. S.G. performed the DFT calculations and interpreted the results. N.V.T. and L.P.Z.

carried out the catalytic evaluation experiments. G.C.V., K.K.A., and I.T. coordinated the research and wrote the final manuscript based on the reports of their collaborators. All authors exchanged opinions concerning the progress of the project and commented on the preparation of the manuscript at all stages. All authors have read and agreed to the published version of the manuscript.

Conflicts of Interest: The authors declare no conflict of interest.

References

1. Afkhami, F.A.; Khandar, A.A.; Mahmoudi, G.; Maniukiewicz, W.; Lipkowski, J.; White, J.M.; Waterman, R.; García-Granda, S.; Zangrando, E.; Bauzái, A.; et al. Synthesis, X-ray characterization, DFT calculations and Hirshfeld surface analysis of Zn(II) and Cd(II) complexes based on isonicotinoylhydrazone ligand. *Cryst. Eng. Comm.* **2016**, *18*, 4587–4596. [CrossRef]

2. Abedi, M.; Yeşilel, O.Z.; Mahmoudi, G.; Bauzá, A.; Lofland, S.E.; Yerli, Y.; Kaminsky, W.; Garczarek, P.; Zaręba, J.K.; Ienco, A.; et al. Tetranuclear manganese(II) complexes of hydrazone and carbohydrazone ligands: Synthesis, crystal structures, magnetic properties, Hirshfeld surface analysis and DFT calculations. *Inorg. Chim. Acta* **2016**, *443*, 101–109. [CrossRef]

3. Romanović, M.Č.; Čobeljić, B.R.; Pevec, A.; Turel, I.; Spasojević, V.; Tsaturyan, A.A.; Shcherbakov, I.N.; Anđelković, K.K.; Milenković, M.; Radanović, D.; et al. Synthesis, crystal structure, magnetic properties and DFT study of dinuclear Ni(II) complex with the condensation product of 2-quinolinecarboxaldehyde and Girard's T reagent. *Polyhedron* **2017**, *128*, 30–37. [CrossRef]

4. Romanović, M.Č.; Milenković, M.R.; Pevec, A.; Turel, I.; Spasojević, V.; Grubišić, S.; Radanović, D.; Anđelković, K.; Čobeljić, B. Crystal structures, magnetic properties and DFT study of cobalt(II) azido complexes with the condensation product of 2-quinolinecarboxaldehyde and Girard's T reagent. *Polyhedron* **2018**, *139*, 142–147. [CrossRef]

5. Pouralimardan, O.; Chamayou, A.-C.; Janiak, C.; Hosseini-Monfared, H. Hydrazone Schiff base-manganese(II) complexes: Synthesis, crystal structure and catalytic reactivity. *Inorg. Chim. Acta* **2007**, *360*, 1599–1608. [CrossRef]

6. Milenković, M.R.; Papastavrou, A.T.; Radanović, D.; Pevec, A.; Jagličić, Z.; Zlatar, M.; Gruden, M.; Vougioukalakis, G.C.; Turel, I.; Anđelković, K.; et al. Highly-efficient *N*-arylation of imidazole catalyzed by Cu(II) complexes with quaternary ammonium-functionalized 2-acetylpyridine acylhydrazone. *Polyhedron* **2019**, *165*, 22–30. [CrossRef]

7. Darmanović, D.; Shcherbakov, I.N.; Duboc, C.; Spasojević, V.; Hanžel, D.; Anđelković, K.; Radanović, D.; Turel, I.; Milenković, M.; Gruden, M.; et al. Combined experimental and theoretical investigation of the origin of magnetic anisotropy in pentagonal bipyramidal isothiocyanato Co(II), Ni(II), and Fe(III) complexes with quaternary-ammonium-functionalized 2,6-diacetylpyridine bisacylhydrazone. *J. Phys. Chem. C* **2019**, *123*, 31142–31155. [CrossRef]

8. Čobeljić, B.; Pevec, A.; Stepanović, S.; Milenković, M.R.; Turel, I.; Gruden, M.; Radanović, D.; Anđelković, K. Structural diversity of isothiocyanato Cd(II) and Zn(II) Girard's T hydrazone complexes in solution and solid state: Effect of H-bonding on coordination number and supramolecular assembly of Cd(II) complex in solid state. *Struct. Chem.* **2018**, *29*, 1797–1806. [CrossRef]

9. Romanović, M.Č.; Čobeljić, B.; Pevec, A.; Turel, I.; Anđelković, K.; Milenković, M.; Radanović, D.; Belošević, S.; Milenković, M.R. Synthesis, crystal structures and antimicrobial activity of azido and isocyanato Zn(II)complexes with the condensation product of 2-quinolinecarboxaldehyde and Girard's T reagent. *J. Coord. Chem.* **2017**, *70*, 2425–2435. [CrossRef]

10. Anđelković, K.; Pevec, A.; Grubišić, S.; Turel, I.; Čobeljić, B.; Milenković, M.R.; Keškić, T.; Radanović, D. Crystal structures and DFT calculations of mixed chloride-azide zinc(II)and chloride-isocyanate cadmium(II) complexes with thecondensation product of 2-quinolinecarboxaldehyde and Girard's Treagent. *J. Mol. Struct.* **2018**, *1162*, 63–70. [CrossRef]

11. Keškić, T.; Čobeljić, B.; Gruden, M.; Anđelković, K.; Pevec, A.; Turel, I.; Radanović, D.; Zlatar, M. What is the nature of interactions of BF_4^-, NO_3^-, and ClO_4^- to Cu(II) complexes with Girard's T hydrazine? When can binuclear complexes be formed? *Cryst. Growth Des.* **2019**, *19*, 4810–4821. [CrossRef]

12. Čobeljić, B.; Turel, I.; Pevec, A.; Jagličić, Z.; Radanović, D.; Anđelković, K.; Milenković, M.R. Synthesis, structures and magnetic properties of octahedral Co(III) complexes of heteroaromatic hydrazones with tetraisothiocyanato Co(II) anions. *Polyhedron* **2018**, *155*, 425–432. [CrossRef]

13. Venkatraman, R.; Fronczek, F.R. *CCDC 1058780: Experimental Crystal Structure Determination*. 2015, Cambridge Crystallographic Data Centre. Available online: https://doi.org/10.5517/CC14JR6M (accessed on 25 May 2020).

14. Lauder, K.; Toscani, A.; Scalacci, N.; Castagnolo, D. Synthesis and reactivity of propargylamines in organic chemistry. *Chem. Rev.* **2017**, *117*, 14091–14200. [CrossRef] [PubMed]

15. Peshkov, V.A.; Pereshivko, O.P.; Van der Eycken, E.V. A walk around the A^3-coupling. *Chem. Soc. Rev.* **2012**, *41*, 3790–3807. [CrossRef] [PubMed]

16. Langston, J.W.; Irwin, I.; Langston, E.B.; Forno, L.S. Pargyline prevents MPTP-induced parkinsonism in primates. *Science* **1984**, *225*, 1480–1482. [CrossRef]

17. Chen, J.J.; Swope, D.M. Clinical pharmacology of rasagiline: A novel, second-generation propargylamine for the treatment of Parkinson disease. *J. Clin. Pharmacol.* **2005**, *45*, 878–894. [CrossRef]

18. Aliaga, M.J.; Ramón, D.J.; Yus, M. Impregnated copper on magnetite: An efficient and green catalyst for the multicomponent preparation of propargylamines under solvent free conditions. *Org. Biomol. Chem.* **2010**, *8*, 43–46. [CrossRef]

19. Pereshivko, O.P.; Peshkov, V.A.; Van der Eycken, E.V. Unprecedented Cu(I)-catalyzed microwave-assisted three-component coupling of a ketone, an alkyne, and a primary amine. *Org. Lett.* **2010**, *12*, 2638–2641. [CrossRef]

20. Vachhani, D.D.; Sharma, A.; Van der Eycken, E.V. Copper-catalyzed direct secondary and tertiary C-H alkylation of azoles through a heteroarene-amine-aldehyde/ketone coupling reaction. *Angew. Chem. Int. Ed.* **2013**, *52*, 2547–2550. [CrossRef] [PubMed]

21. Cheng, M.; Zhang, Q.; Hu, X.; Li, B.; Ji, J.; Chan, A. Gold-catalyzed direct intermolecular coupling of ketones, secondary amines, and alkynes: A facile and versatile access to propargylic amines containing a quaternary carbon center. *Adv. Synth. Catal.* **2011**, *353*, 1274–1278. [CrossRef]

22. Suzuki, Y.; Naoe, S.; Oishi, S.; Fujii, N.; Ohno, H. Gold-catalyzed three-component annulation: Efficient synthesis of highly functionalized dihydropyrazoles from alkynes, hydrazines, and aldehydes or ketones. *Org. Lett.* **2011**, *14*, 326–329. [CrossRef] [PubMed]

23. Meyet, C.E.; Pierce, C.J.; Larsen, C.H. A single Cu(II) catalyst for the three-component coupling of diverse nitrogen sources with aldehydes and alkynes. *Org. Lett.* **2012**, *14*, 964–967. [CrossRef] [PubMed]

24. Pierce, C.J.; Larsen, C.H. Copper(II) catalysis provides cyclohexanone-derived propargylamines free of solvent or excess starting materials: Sole by-product is water. *Green Chem.* **2012**, *14*, 2672–2676. [CrossRef]

25. Palchak, Z.L.; Lussier, D.J.; Pierce, C.J.; Larsen, C.H. Synthesis of tetrasubstituted propargylamines from cyclohexanone by solvent-free copper(II) catalysis. *Green Chem.* **2015**, *17*, 1802–1810. [CrossRef]

26. Pierce, C.J.; Nguyen, M.; Larsen, C.H. Copper/titanium catalysis forms fully substituted carbon centers from the direct coupling of acyclic ketones, amines, and alkynes. *Angew. Chem. Int. Ed.* **2012**, *51*, 12289–12292. [CrossRef]

27. Tang, X.; Kuang, J.; Ma, S. CuBr for KA^2 reaction: En route to propargylic amines bearing a quaternary carbon center. *Chem. Commun.* **2013**, *49*, 8976–8978. [CrossRef]

28. Cai, Y.; Tang, X.; Ma, S. Identifying a highly active copper catalyst for KA^2 reaction of aromatic ketones. *Chem. Eur. J.* **2016**, *22*, 2266–2269. [CrossRef]

29. Vougioukalakis, G.C.; Grubbs, R.H. Ruthenium-Based Heterocyclic Carbene-Coordinated Olefin Metathesis Catalysts. *Chem. Rev.* **2010**, *110*, 1746–1787. [CrossRef]

30. Pinaka, A.; Vougioukalakis, G.C. Using sustainable metals to carry out "green" transformations: Fe- and Cu-catalyzed CO_2 monetization. *Coord. Chem. Rev.* **2015**, *288*, 69–97. [CrossRef]

31. Tzouras, N.V.; Stamatopoulos, I.K.; Papastavrou, A.T.; Liori, A.A.; Vougioukalakis, G.C. Sustainable metal catalysis in C-H activation. *Coord. Chem. Rev.* **2017**, *343*, 25–138. [CrossRef]

32. Liori, A.; Stamatopoulos, I.K.; Papastavrou, A.T.; Pinaka, A.; Vougioukalakis, G.C. A novel, sustainable, user-friendly protocol for the Pd-free Sonogashira coupling reaction. *Eur. J. Org. Chem.* **2018**, *2018*, 6134–6139. [CrossRef]

33. Papastavrou, A.T.; Pauze, M.; Gomez-Bengoa, E.; Vougioukalakis, G.C. Unprecedented multicomponent organocatalytic synthesis of propargylic esters via CO_2 activation. *Chem. Cat. Chem.* **2019**, *11*, 5379–5386.

34. Tzouras, N.V.; Neofotistos, S.P.; Vougioukalakis, G.C. Zn-catalyzed multicomponent KA^2 coupling: One-pot assembly of propargylamines bearing tetrasubstituted carbon centers. *ACS Omega* **2019**, *4*, 10279–10292. [CrossRef]

35. Addison, A.W.; Rao, T.N.; Reedijk, J.; Van Rijn, J.; Verschoor, G.C. Synthesis, structure, and spectroscopic properties of copper(II) compounds containing nitrogen–sulphur donor ligands; the crystal and molecular structure of aqua [1,7-bis(*N*-methylbenzimidazol-2′-yl)-2,6-dithiaheptane]copper(II) perchlorate. *J. Chem. Soc. Dalton Trans.* **1984**, 1349–1356. [CrossRef]

36. Moroz, Y.S.; Sliva, T.Y.; Kulon, K.; Kozłowski, H.; Fritsky, I.O. Di-chlorido{2-hy-droxy-imino-*N*′-[1-(2-pyrid-yl)ethylidene]propanohydrazide-$\kappa^3 N,N',O$}zinc(II) hemihydrate. *Acta Cryst.* **2008**, *E64*, m353–m354.

37. Chaur, M.N. Di-chlorido{(E)-4-di-methyl-amino-*N*′-[(pyri-din-2-yl)methyl–idene-κN]benzo-hydrazide-κO}zinc. *Acta Cryst.* **2013**, *E69*, m27.

38. Reena, T.A.; Seena, E.B.; Prathapachandra Kurup, M.R. Zinc(II) complexes derived from di-2-pyridyl ketone N^4-phenyl-3-semicarbazone: Crystal structures and spectral studies. *Polyhedron* **2008**, *27*, 3461–3466. [CrossRef]

39. Despaigne, A.A.R.; Da Silva, J.G.; Do Carmo, A.C.M.; Sives, F.; Piro, O.E.; Castellano, E.E.; Beraldo, H. Copper(II) and zinc(II) complexes with 2-formylpyridine-derived hydrazones. *Polyhedron* **2009**, *28*, 3797–3803. [CrossRef]

40. Li, L.; Zhang, Y.Z.; Liu, E.; Yang, C.; Golen, J.A.; Rheingold, A.L.; Zhang, G. Synthesis and structural characterization of zinc(II) and cobalt(II) complexes based on multidentatehydrazone ligands. *J. Mol. Struct.* **2016**, *1110*, 180–184. [CrossRef]

41. Steiner, T. The Hydrogen Bond in the Solid State. *Angew. Chem. Int. Ed.* **2002**, *41*, 48–76. [CrossRef]

42. Neofotistos, S.P.; Tzouras, N.V.; Pauze, M.; Gomez-Bengoa, E.; Vougioukalakis, G.C. Manganese-Catalyzed Multicomponent Synthesis of Tetrasubstituted Propargylamines: System Development and Theoretical Study. *Adv. Synth. Catal.* **2020**, *362*. [CrossRef]

43. Kosar, B.; Albayrak, C. Spectroscopic investigations and quantum chemical computational study of (*E*)-4-methoxy-2-[(p-tolylimino)methyl]phenol. *Spectrochim. Acta A* **2011**, *78*, 160–167. [CrossRef] [PubMed]

44. Rauk, A. *Orbital Interaction Theory of Organic Chemistry*, 2nd ed.; John Wiley & Sons: New York, NY, USA, 2001; p. 34.

45. Tabares-Mendoza, C.; Guadarrama, P. Predicting the catalytic efficiency by quantum-chemical descriptors: Theoretical study of pincer metallic complexes involved in the catalytic Heck reaction. *J. Organomet. Chem.* **2006**, *691*, 2978–2986. [CrossRef]

46. Geerlings, P.; De Proft, F.; Langenaeker, W. Conceptual Density Functional Theory. *Chem. Rev.* **2003**, *103*, 1793–1874. [CrossRef]

47. Govindarajan, M.; Karabacak, M.; Periandy, S.; Tanuja, D. Spectroscopic (FT-IR, FT-Raman, UV and NMR) investigation and NLO, HOMO–LUMO, NBO analysis of organic 2,4,5-trichloroaniline. *Spectrochim. Acta A Mol. Biomol. Spectrosc.* **2012**, *97*, 231–245. [CrossRef] [PubMed]

48. Domingo, L.R.; Ríos-Gutiérrez, M.; Pérez, P. Applications of the Conceptual Density Functional Theory Indices to Organic Chemistry Reactivity. *Molecules* **2016**, *21*, 748. [CrossRef] [PubMed]

49. Zhan, C.G.; Nichols, J.A.; Dixon, D.A. Ionization Potential, Electron Affinity, Electronegativity, Hardness, and Electron Excitation Energy: Molecular Properties from Density Functional Theory Orbital Energies. *J. Phys. Chem. A* **2003**, *107*, 4184–4195. [CrossRef]

50. Fukui, K. Role of Frontier Orbitals in Chemical Reactions. *Science* **1982**, *218*, 747. [CrossRef]

51. Otwinowsky, Z.; Minor, W. Processing of X-ray Diffraction Data Collected in Oscillation Mode. *Methods Enzymol.* **1997**, *276*, 307–326.

52. CrysAlis PRO. *Oxford Diffraction*; Oxford Diffraction Ltd.: Yarnton, UK, 2009.

53. Altomare, A.; Cascarano, G.; Giacovazzo, C.; Guagliardi, A. Completion and refinement of crystal structures with SIR92. *J. Appl. Crystallogr.* **1993**, *26*, 343–350. [CrossRef]

54. Sheldrick, G.M. A short history of SHELX. *Acta Crystallogr.* **2008**, *A64*, 112–122. [CrossRef]

55. Frisch, M.J.; Trucks, G.W.; Schlegel, H.B.; Scuseria, G.E.; Robb, M.A.; Cheeseman, J.R.; Scalmani, G.; Barone, V.; Mennucci, B.; Petersson, G.A.; et al. *Gaussian 09 (Revision D.01)*; Gaussian, Inc.: Wallingford, CT, USA, 2009.

56. Becke, A.D. Density-functional thermochemistry. III. The role of exact exchange. *J. Chem. Phys.* **1993**, *98*, 5648. [CrossRef]

57. Lee, C.; Yang, W.; Parr, R.G. Development of the Colle-Salvetti correlation-energy formula into a functional of the electron density. *Phys. Rev. B Condens. Matter* **1988**, *37*, 785. [CrossRef] [PubMed]

58. Hehre, J.; Ditchfield, R.; Pople, J.A. Self–Consistent Molecular Orbital Methods. XII. Further Extensions of Gaussian–Type Basis Sets for Use in Molecular Orbital Studies of Organic Molecules. *J. Chem. Phys.* **1972**, *56*, 2257–2261. [CrossRef]

59. Hariharan, P.C.; Pople, J.A. The influence of polarization functions on molecular orbital hydrogenation energies. *Theor. Chim. Acta* **1973**, *28*, 213–222. [CrossRef]

60. Caricato, M.; Mennucci, B.; Tomasi, J.; Ingrosso, F.; Cammi, R.; Corni, S.; Scalmani, G. Formation and relaxation of excited states in solution: A new time dependent polarizable continuum model based on time dependent density functional theory. *J. Chem. Phys.* **2006**, *124*, 124520–124532. [CrossRef]

61. Institute of Physics Belgrade. *PARADOX Cluster User Guide v2.1: PARADOX IV Cluster*; Institute of Physics Belgrade: Belgrade, Serbia, 2018.

Sample Availability: Samples of the compounds are not available from the authors.